Current Research in Structural Biology 3 (2021) 112–120

Contents lists available at ScienceDirect

Current Research in Structural Biology

journal homepage: www.journals.elsevier.com/current-research-in-structural-biology

De novo crystal structure determination of double stranded RNA binding domain using only the sulfur anomalous diffraction in SAD phasing

Beatriz Gomes Guimarães [a,1], Béatrice Golinelli-Pimpaneau [b,*]

[a] Synchrotron Soleil, L'Orme des Merisiers, Saint-Aubin 91190 Gif-sur-Yvette, France
[b] Laboratoire de Chimie des Processus Biologiques, UMR 8229 CNRS, Collège de France, Sorbonne Université, 11 Place Marcelin Berthelot, 75005 Paris, France

ARTICLE INFO

Keywords:
de novo structure determination
Sulfur SAD-Phasing
S-SAD
Multi-orientation
Double stranded RNA binding Domain

ABSTRACT

Single-wavelength anomalous dispersion (SAD)-phasing using sulfur as the unique anomalous scatterer is a powerful method to solve the phase problem in protein crystallography. However, it is not yet widely used by non-expert crystallographers. We report here the structure determination of the double stranded RNA binding domain of human dihydrouridine synthase using the sulfur-SAD method and highly redundant data collected at 1.8 Å ("off-edge"), at which the estimated overall anomalous signal was 1.08%. High multiplicity data were collected on a single crystal rotated along the ϕ or ω axis at different κ angles, with the primary beam intensity being attenuated from 50% to 95%, compared to data collection at 0.98 Å, to reduce radiation damage. *SHELXD* succeeded to locate 14 out 15 sulfur sites only using the data sets recorded with highest beam attenuation, which provided phases sufficient for structure solving. In an attempt to stimulate the use of sulfur-SAD phasing by a broader community of crystallographers, we describe our experimental strategy together with a compilation of previous successful cases, suggesting that sulfur-SAD phasing should be attempted for determining the *de novo* structure of any protein with average sulfur content diffracting better than 3 Å resolution.

1. Introduction

The general method for *de novo* solving the crystal structure of a protein is to prepare the selenomethionylated protein and use the anomalous signal of Se atoms to determine experimental phases using the multiple-wavelength anomalous dispersion (MAD) (Hendrickson, 1991) or single-wavelength anomalous dispersion (SAD) methods (Hendrickson, 2014). Compared to MAD, only one data set at or around the absorption edge of the anomalous atom ("anomalous" data set) is needed for SAD, which minimizes the effect of radiation damage. In addition, a so-called "native" data set may be used, in some cases, for final structure refinement. Although successfully used in a large number of cases, Se-SAD phasing has some drawbacks. First, it requires Se-labeling of the protein. Second, it is never known in advance if expression and solubility of the selenomethionylated protein will be sufficient and if crystallization will occur in the same conditions as the native protein.

In contrast, the native SAD method can be used to derive experimental phases directly from native protein crystals without the need of additional derivatives. Indeed, proteins contain different types of atoms that can be used as anomalous scatterers, although much weaker than selenium. In particular, sulfur is the heaviest atom in most native proteins, present within the cysteine and methionine amino acids that compose the polypeptide chain. In addition, other atoms such as Ca, Cl, Mg, K, Na, are occasionally - and sometimes fortuitously (Hegde et al., 2017) - found within the protein crystal, as determined by the X-ray fluorescence emission spectrum. Their anomalous signal can be exploited together with the sulfur signal for successful native SAD phasing (Dauter et al., 1999; Goulet et al., 2010; Liu et al., 2012; Doutch et al., 2012; Liu and Hendrickson, 2015; Rose et al., 2015; Weinert et al., 2015; Olieric et al., 2016; Olczak and Cianci, 2018).

Crambin was the first protein whose structure was solved by sulfur-SAD (Hendrickson and Teet, 1981). Favorable factors included a large (15%) sulfur content (i. e. percentage of sulfur-containing residues in the polypeptide chain), the presence of disulfide bonds, which account as "super-sulfur" sites (Kraatz et al., 2018), and diffraction to high resolution (1.5 Å). Later developments in diffraction hardware and crystallographic programs, together with extended and judicious use of data statistics (Foos et al., 2019; Assmann et al., 2020) made native-SAD phasing accessible to numerous other proteins (Liu et al., 2012; Liu and Hendrickson, 2015; Rose et al., 2015). The absorption edge of sulfur

* Corresponding author.
E-mail address: beatrice.golinelli@college-de-france.fr (B. Golinelli-Pimpaneau).
[1] present address: Carlos Chagas Institute, Oswaldo Cruz Foundation, Curitiba, Paraná, Brazil

https://doi.org/10.1016/j.crstbi.2021.05.002
Received 26 March 2021; Received in revised form 7 May 2021; Accepted 31 May 2021

is λ = 5.02 Å. At such a high wavelength, where anomalous scattering is optimal, radiation damage is enhanced and X-ray absorption becomes severe. Hence, as a compromise between higher anomalous signal at low energy and lower noise at high energy, sulfur-SAD phasing is usually carried out "off-edge" at shorter wavelengths (1.5–3 Å). Home-source with Cu (λ = 1.54 Å) (Sarma and Karplus, 2006) or Cr (λ = 2.29 Å) radiations (Watanabe, 2006) have been used to solve the structure of large and well-diffracting crystals, whereas synchrotron beamlines have been developed to optimize beam stability and minimize X-ray absorption effects for native SAD data collection in more difficult cases (Doutch et al., 2012; Weinert et al., 2015; Wang et al., 2006; Basu et al., 2019a; De Sanctis et al., 2016; Cianci et al., 2017). Moreover, the development of pixel array detectors that operate in single photon counting mode such as the Pilatus (Broennimann et al., 2006) has been a breakthrough in macromolecular crystallography by enabling noise-free detection and novel data-acquisition modes.

To accurately measure the very weak sulfur anomalous signal at standard synchrotron beamlines and optimize the signal-to-noise ratio, highly redundant diffraction data are needed (Liu et al., 2012, 2014; Doutch et al., 2012; Ramagopal et al., 2003; Cianci et al., 2008), which may, however, increase radiation damage. Among the various synchrotron data-collection strategies that have been proposed to optimize native-SAD (Olieric et al., 2016) - including sulfur-SAD - phasing, the use of a long-wavelength (2.7 Å) over 1.9 Å (Cianci et al., 2016; Banerjee et al., 2016; Basu et al., 2019b) was shown to be advantageous for 100 μm or smaller crystals (Basu et al., 2019b; Liebschner et al., 2016). Moreover, successful native SAD phasing was achieved in several difficult cases using low X-ray dose, high redundancy and multi-orientations data collection of multiple crystals (Liu et al., 2012, 2014; Assmann et al., 2020; Banerjee et al., 2016; Akey et al., 2014; El Omari et al., 2014; Klinke et al., 2015), or even a single crystal (Weinert et al., 2015; Basu et al., 2019a,b), which obviously removes the problem of non-isomorphism between various crystals. The latest technical advances include solution-free mounting systems to minimize X-ray absorption at long-wavelengths (Yu et al., 2020) and assembly of numerous partial single-crystal data sets from microcrystals with sizes less than 10 μm (Cianci et al., 2019; Guo et al., 2019; Nass et al., 2020). Despite these improvements, native SAD phasing is still not yet a routine method for successful structure solution (Rose et al., 2015; Basu et al., 2019a) because success is not only dependent on the content in anomalous scattering atoms but also on the crystal features, with a high diffracting power and high symmetry being advantageous.

In several cases, native SAD phasing was achieved using atoms other than S as scatterers, such as Ca, Cl, K, Na, Mg, which were constitutive of the protein or originated fortuitously from the crystallization solution (Dauter et al., 1999; Weinert et al., 2015; Olieric et al., 2016; Basu et al., 2019a, 2019b; Mueller-Dieckmann et al., 2007). Because the anomalous scattering factors f'' of the atoms that are heavier than S (Ca, Cl, K) are higher than that of sulfur in the 1–2 Å wavelength range used at synchrotrons (see Fig. 1 in Mueller-Dieckmann et al., 2007), these atoms had often an important contribution to the phasing success (Goulet et al., 2010; Rose et al., 2015; Weinert et al., 2015; Olieric et al., 2016). Here, we review the recent cases, described in the literature, where native SAD phasing was used successfully using no atoms heavier than sulfur as anomalous scatterers (Table 1). Difficult cases include crystals belonging to low symmetry space groups (Basu et al., 2019a; Banerjee et al., 2016; Klinke et al., 2015), diffracting at poor resolution (Liu et al., 2014; Cianci et al., 2016; Basu et al., 2019b; Akey et al., 2014; El Omari et al., 2014; Klinke et al., 2015) with an extremely low sulfur content (Basu et al., 2019a; Gorgel et al., 2015) or large substructure (Basu et al., 2019b; Akey et al., 2014; Klinke et al., 2015). We also report our experience, where several data sets collected in various goniometer orientations on a single

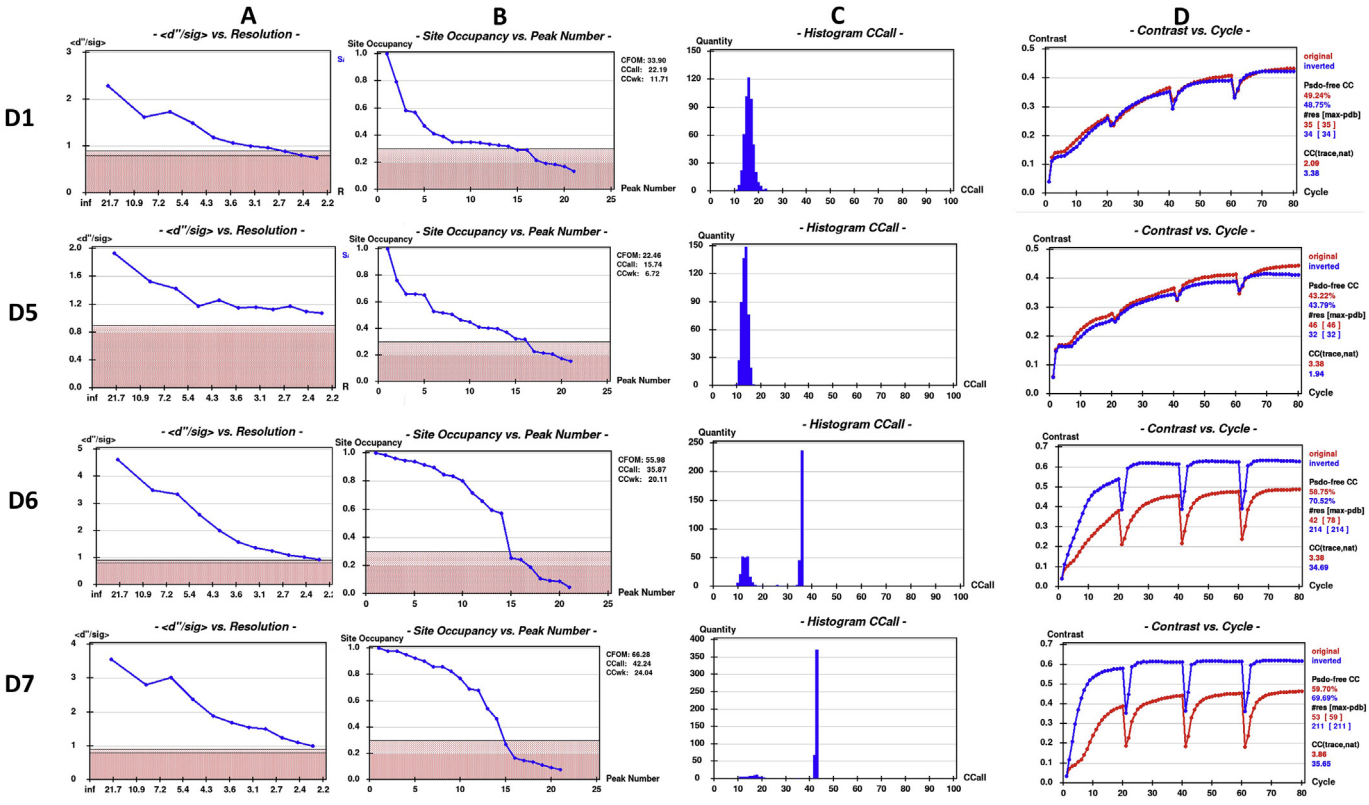

Fig. 1. Analysis of substructure determination using the D1, D5, D6 and D7 data sets. **A** Profiles of the anomalous signals <ΔF>/σ <F> as a function of resolution, as determined by *SHELXC*. **B** Plot of site occupancy versus peak heights for the top 25 peaks observed in the Bijvoet difference Fourier maps for the search of 15 S sites with *SHELXD*. **C** Histogram of the CC_{all} correlation coefficients between observed and calculated Bijvoet differences out of 500 tries of *SHELXD*. **D** Contrast analysis of original and inverted hands versus cycle during phasing with *SHELXE*.

Table 1
Protein structures solved using synchrotron radiation and only the sulfur anomalous signal in SAD phasing. Particular features (such as low symmetry, poor diffraction, low solvent content, large asymmetric unit content) that make structure determination by S-SAD more challenging are indicated in bold. Examples of other structures solved by native SAD using sulfur and another scattering atom can be found in Table 1 of Olczak and Cianci, 2018 and Supplementary Tables 1 of Weinert et al. (2015) and Gorgel et al. (2015).

Protein PDB code	S-SAD λ (Å) E (keV)	Diffraction limit (Å) for native data set	Space group	Sulfur content	Number of Cys + Met in asymmetric unit [a]	Number of residues in asymmetric unit (kDa)	Solvent %	Collection strategy	Total rotation range (°)/redundancy	Predicted Bijvoet ratio ΔF/F (%)[b]	substructure determination: initial number of sites and resolution cutoff (Å)	N° of crystals	Crystal size (μm^3)	Beamline	Reference
Lam16A 2cl2	1.775 (7.0)	1.34	$P2_12_12_1$	4.4	13 (including 4 SS bridges)	298 (36)	**35**	Single orientation of a unique crystal	500/19.0	**1.1**	13 (2.5)	1	500 × 500 x 500	ID14-4, ESRF Grenoble, France	Vasur et al. (2006)
ORF 1382 from *Archaeoglobus fulgidus* 3o3k	1.9 (6.25)	2.3	$P4_2$	5.3	4	95 (11.1)	54.4	Multiple orientations of a single crystal	720/25	1.4	4 (?)	1	?	22ID SER-CAT, Advanced Photon Source, Argonne National Laboratory USA	Zhu et al. (2012)
flavivirus NS1 4tpl	1.746 (7.1)	**2.9**	P321	4.8	**17 x 2 (including 12 SS bridges)**	**377 x 2 (85)**	72.5	Multiple crystals Inversed beam	28 × 180/184.1	1.3	31 (5.2)	**28**	50 x 50 x 150	23ID-D Advanced Photon Source, Argonne National Laboratory USA	Akey et al. (2014)
Thiamine transporter ThiT 4tkr	2.066 (6.0)	**3.0**	$P3_121$	4.3	8 × 2	184 × 2 (40.3)	69.0	Multiple crystals Inversed beam	2600/140.2	1.5	15 (?)	5	75 x 75 x 75	NSLS X4A, Brookhaven National Laboratory USA	Liu et al. (2014)
EGFR kinase domain 4tks	2.066 (6.0)	**3.2**	I23	4.7	15	318 (36.8)	64.3	Multiple crystals Inversed beam	2160/254.1	1.5	15 (?)	4	100 × 100 x 100	NSLS X4A, Brookhaven National Laboratory USA	Liu et al. (2014)
Nter domain of the ectodomain of HCV E1 4uoi	1.77 (7.0)	**3.5**	$P4_12_12$	5.1	4 × 6 (including 10 SS bridges)	79 × 6 (57.6)	52	Multiple crystals Inversed beam	90 × 32/121.5	**1.1**	12 (7)	**32**	110 × 30 x 10	I04, Diamond Light Source England	El Omari et al. (2014)
D29 construct of CopN microtubule-destabilizing protein 4p3z	1.9 (6.525)	1.77	$P2_12_12_1$	2.6	11 (including four sulfate ions)	424 (46.4)	**32**	Multiple orientations of a single crystal	?/10.6	1.4	7 (?)	1	?	PX1 SOLEIL France	Nawrotek et al. (2014)
Brucellus abortus Histidine kinase domain 5epv	1.8 (6.888)	**2.9**	**$P2_1$**	4.5	**10 x 4**	**242 x 4 (108)**	52	Multiple orientations of multiple crystals	4000/35.6	**1.2**	27/32 (4)	3	400 × 100 x 50	PX1 SOLEIL France	Klinke et al. (2015)
Pilin PilBac1 4us7	1.8 (6.888)	1.96	I222	**2.2**	3 × 2 (including 2 SS bridges and 2 sulfate ions)	89 × 2 (19.8)	62.4	Multiple orientations of a single crystal	?/**5.5**	**0.9**	5 (?)	1	70 x 70 x 700	BL-14.1, BESSY II, Germany	Gorgel et al. (2015)
hypothetical protein pf1771 4wbx	2.066 (6.0)	2.5	F222	3.3	13	395 (44.0)	53	Low-dose & Multiple	360 × 5/62.7	**1.3**	13 (3.7)	1	150 × 100 x 100	X06DA Swiss Light	Weinert et al. (2015)

(*continued on next page*)

Table 1 (*continued*)

Protein PDB code	S-SAD λ (Å) E (keV)	Diffraction limit (Å) for native data set	Space group	Sulfur content	Number of Cys + Met in asymmetric unit [a]	Number of residues in asymmetric unit (kDa)	Solvent %	Collection strategy	Total rotation range (°)/redundancy	Predicted Bijvoet ratio ΔF/F (%)[b]	substructure determination: initial number of sites and resolution cutoff (Å)	N° of crystals	Crystal size (μm^3)	Beamline	Reference
								orientations of a single crystal						Source, Switzerland	
Human centromere protein M CENP-M 4wau	2.066 (6.0)	2.2	P3	4.5	7 × 2	155 × 2 (34.1)	55.3	Low-dose & Multiple orientations of a single crystal	720 × 5 +2880/140.4	1.5	14 (2.7)	1	100 × 100 x 150	X06DA Swiss Light Source, Switzerland	Weinert et al. (2015)
Cdc-23 Nter 5ftp	2.7 (4.6)	**3.1**	$P4_3$	3.9	11 × 2	282 × 2 (65.4)	53	Long wavelength 2 data sets from a single crystal	720/27.8	2.2	17 (4)	1	~50 × 50 x 100	P13 DESY Germany	Cianci et al. (2016)
Lili-Mip 4nyr	2.7 (4.6)	1.2	**P1**	3.05	5 (including 2 SS bridges)	164 (18.7)	42.5	Long wavelength Multiple crystals	7 × 720/23	2.0	?	7	10 x 10 x 30 in vivo grown crystals	BL-1A, Photon Factory, Japan	Banerjee et al. (2016)
Helicase Sen1 6i59	2.7 (4.6)	**2.95**	$P2_12_12$	4.4	**31**	**749 (85.1)**	61.6	Long wavelength Multiple orientations of a single crystal	1440/49.1	2.3	22 (3.3)	1	220 × 100 x 50	BL-1A KEK Photon Factory, Japan	Basu et al. (2019b)
Streptavidin-biotin (SavB) 6m9b	2.07 (6.0)	1.55	**$P2_1$**	**0.8**	1 × 4 (4 S from biotin)	127 × 4 (53.1)	46.5	Low-dose Multiple orientations of a single crystal	14 × 360/39.0	**0.6**	4 (?)	1	50 × 150 x 200	X06DA Swiss Light Source, Switzerland	Basu et al. (2019a)
Thaumatin 6o8a	2.48 (5.0)	2.6	$P4_12_12$	8.2	17 (including 8 SS bridges)	207 (22.2)	56.3	Polyimide well mounts & iterative frame rejection	1381 × 20/322.7	2.8	?	**1381**	**Micro-crystals < 10 µm**	FMX (NSLS-II), Brookahven National Lab, NY, USA	Guo et al. (2019)
Bacteriophage T4 Spackle 6x6o	1.653 (7.0)	1.52	I222	7.2	6 × 2 (including 2 SS bridges)	83 × 2 (19.5)	**28.2**	Single orientation of a single crystal	720/21.9	1.5	12 (2.2)	1	?	24-ID-C NE-CAT Advanced Photon Source, Argonne National Laboratory USA	Shi et al. (2020)
Eisenia hydrolysis protein (EHEP) Not deposited at the PDB	2.1 (5.9)	1.2	$P2_12_12_1$	9.5	20	209 (22.6)	32.7	Solution-less crystal mounting Multiple orientations of a single crystal	8 × 720/105	2.3	20 (?)	1	270 × 50 x 50	BL17A, Photon factory, Japan	Yu et al. (2020) Sun et al. (2020)
dsRBD of DUS 4WFT	1.8 (6.888)	1.77	$P4_3$	4.1	5 × 3	119 × 3 (41.1)	41.8	Low-dose & Multiple orientations of a single crystal	See text	**1.08**	See text	1	150 × 150 x 100	PX1 SOLEIL France	This paper

? not indicated in the original paper.

[a] Except N-terminal methionine.

[b] The expected Bijvoet ratio of the mean anomalous difference to the mean amplitude expected in the data at a given wavelength can be estimated by the formula= $(2N_A)^{1/2}$ x f"/$(346\ N_R)^{1/2}$, where N_A and N_R are the number of anomalous atoms and number of protein residues in the asymmetric unit, respectively, and f" is the atomic scattering factor of the anomalous atom (here sulfur), which depends on the wavelength (Hendrickson and Teet, 1981). If anomalous scatterers form a group (e.g. a disulfide or a metal cluster), this changes the dependence of the anomalous signal on resolution (Banumathi et al., 2003). The theoretical Bijvoet ratios for S-SAD structures from the PDB range from 0.6 to 4.1%, with an average of 1.4% (Rose et al., 2015). Bijvoet ratios below the average number have been highlighted.

Table 2
Data collection and reduction statistics of each data set of the four crystals D1, D5, D6 and D7.

Crystal	D1	D1	D1	D5	D5	D5	D5	D6	D6	D6	D6	D7	D7	D7	D7	D7
Data set name	native	sad1	sad2	native	sad1	sad2	sad3	native	sad1	sad2	sad3	sad1	sad2	sad3	sad4	sad5
Rotation axis	ϕ	ϕ	ω	ϕ	ϕ	ω	ω	ϕ	ϕ	ϕ	ϕ	ϕ	ϕ	ϕ	ω	ω
κ angle °	0	0	15	0	0	15	−15	0	0	15	−20	0	20	−20	−20	20
Unit cell parameters (Å) a, c	55.5 115.3	55.6 115.4	55.7 115.7	55.5 115.2	55.6 115.3	55.8 115.7	55.8 115.9	55.5 115.2	55.5 115.3	55.5 115.3	55.5 115.3	55.4 115.0	55.4 115.1	55.4 115.1	55.4 115.1	55.4 115.1
Transmission (%)	50	50	50	40	40	40	40	30	20	20	20	5	5	5	5	5
Number of frames	600	800	900	500	800	900	900	900	2000	2000	2000	2500	2500	2500	900	900
Resolution (Å) (high resolution shell)	50–1.87 (1.98–1.87)	50–2.2 (2.33–2.20)	50–2.2 (2.33–2.20)	50–1.69 (1.79–1.69)	50–2.2 (2.33–2.20)	50–2.2 (2.33–2.20)	50–2.2 (2.33–2.20)	50–2.06 (2.18–2.06)	50–2.2 (2.33–2.20)	50–2.2 (2.33–2.20)	50–2.2 (2.33–2.20)	50–2.2 (2.33–2.20)	50–2.2 (2.33–2.20)	50–2.2 (2.33–2.20)	50–2.2 (2.33–2.20)	50–2.2 (2.33-2.20)
Measurements	128676 (20494)	98820 (13852)	111618 (15430)	146988 (23297)	99638 (34465)	113399 (15862)	114873 (15953)	148537 (23461)	255226 (37097)	254989 (36990)	236275 (33731)	310021 (36311)	318759 (46076)	317789 (46374)	115449 (16966)	114414 (16938)
Unique reflections	28771 (4612)	34083 (5286)	34934 (5455)	11988 (5489)	13864 (5347)	35031 (5530)	35236 (5555)	21618 (3457)	35105 (5673)	35126 (5698)	34949 (5600)	34810 (5630)	34841 (5652)	34840 (5652)	34666 (5559)	34622 (5556)
Multiplicity	6.3 (6.2)	2.9 (2.6)	3.2 (2.8)	3.8 (3.7)	2.9 (2.6)	3.2 (2.9)	3.3 (2.9)	6.9 (6.8)	7.3 (6.5)	7.3 (6.5)	6.8 (6.0)	8.9 (6.45)	9.1(8.1)	9.1 (8.2)	3.3 (3.05)	3.3 (3.05)
Completeness (%)	99.6 (99.2)	97.0 (92.8)	98.3 (94.4)	99.3 (99.0)	98.1 (94.1)	98.6 (95.5)	98.8 (95.5)	99.9 (99.7)	99.9 (99.5)	100 (99.9)	99.8 (99.1)	99.9 (99.6)	100 (99.9)	100 (99.9)	99.4 (98.8)	99.4 (98.9)
R_{meas}	3.9 (21.8)	3.9 (14.8)	6.0 (33.3)	3.5 (42.1)	3.0 (10.0)	4.3 (25.1)	6.1 (41.1)	3.9 (24.6)	4.3 (22.9)	4.3 (23.0)	4.4 (22.8)	4.9 (13.7)	5.6 (13.9)	4.4 (13.4)	4.4 (13.4)	4.9 (13.5)
I/σ(I)	25.84 (6.94)	22.98 (7.03)	16.34 (3.54)	23.5 (3.4)	29.93 (10.6)	20.3 (4.5)	18.00 (2.77)	38.25 (8.25)	36.34 (8.01)	36.6 (7.96)	34.8 (7.8)	32.71 (11.46)	29.28 (12.78)	35.8 (13.5)	21.6 (8.1)	19.63 (8.04)
ΔF/σ(ΔF)	–	2.134 (1.070)	2.156 (0.982)	–	2.172 (1.280)	2.104 (0.900)	1.803 (0.671)	–	1.162 (0.827)	1.185 (0.867)	1.165 (0.860)	1.088 (0.856)	1.057 (0.884)	1.144 (0.892)	0.989 (0.852)	0.999 (0.836)
ΔF/σ(ΔF) at 2.9 Å [a]	–	2.545	2.744	–	2.561	2.542	2.482	–	1.158	1.198	1.109	1.079	1.072	1.140	1.020	1.021

[a] ΔF/σ(ΔF) is the average anomalous signal from data truncated to dmin = 2.9 Å.

well-diffracting crystal of the double stranded RNA binding domain (dsRBD) of human dihydrouridine synthase hdus2 were used for successful sulfur-SAD phasing. This average case (tetragonal space group, diffraction to 1.8 Å, average number of sulfur atoms), together with the previous published literature, should encourage non-expert crystallographers to attempt sulfur-SAD phasing for *de novo* structure determination of proteins containing only light atoms, using only the sulfur anomalous signal.

2. Method: crystallization and data collection

The 13.7 kDa C-terminal domain (residues 345 to 457; 113 amino acids) of hdus2 dsRBD was expressed with a C-terminal 6-histidines tag. Crystals (~150 × 150 × 100 μm^3) were obtained at 18 °C in hanging-drops by vapor diffusion by mixing 1 μl of a solution containing 34 mg ml^{-1} protein in 25 mM Tris-HCl pH 8.0, 0.15 M NaCl with 1 μl of a 1 ml reservoir solution (28% PEG MMG, 2000, 0.1 sodium acetate, 0.1 M HEPES pH 7.5), as reported (Bou-Nader et al., 2015). Crystals were soaked for a few minutes in the same solution containing 25% glycerol before flash freezing in liquid nitrogen. Diffraction data were collected on the PROXIMA 1 beam line at the SOLEIL synchrotron (Saint Aubin, France) using a Pilatus detector (Broennimann et al., 2006) and an oscillation angle of 0.2° per frame with an exposure time of 0.2 s. The beamline was configured to provide a focused X-ray beam of 125 × 65 μm^2 and a photon flux of ~5.8 × 10^{11} and 7 × 10^{11} photons/s at ~7 keV and ~12 keV, respectively.

A so-called "native" data set, called D1, was collected at λ = 0.98 Å (12.7 keV) and 100 K. Then, using the same crystal, various consecutive "SAD" data sets were collected at a wavelength of 1.8 Å (6.89 keV) by rotating the crystal around the ϕ or ω axis at different fixed κ angles. Given the crystals dimensions and beam size, the crystal was not translated between the different data sets. Data were processed with *XDS* and merged with *XSCALE* (Kabsch, 2010) using the native data set as a reference, the *hkl* and *-h-k-l* reflections in an anomalous pair being treated as separate reflections during scaling and merging. The graphical user interface *HKL2MAP* (Pape and Schneider, 2004) was used for phasing with the *SHELX* programs (Usón and Sheldrick, 2018). The heavy-atom substructure was solved with *SHELXD* (Schneider and Sheldrick, 2002) using 500 trials and testing different resolution cut-offs. *SHELXE* (Sheldrick, 2002) was used to select the correct hand and attest for successful phasing. The substructures were refined and completed with *PHASER* (Adams et al., 2010) using all data. Phases were generated and density modification was performed using 5 cycles of *PARROT* (Cowtan, 2010) to improve phases. *BUCCANEER* (Cowtan, 2006) (5 cycles) was used for automated model building. The final data and refinement statistics for the native and anomalous data sets were previously reported in Table S1 in Bou-Nader et al. (2015) and deposited in the PDB (code 4WFT).

3. Results and discussion

Dihydrouridine synthases (DUS) catalyze the reduction of uridine to dihydrouridine mainly in the D-loop of tRNAs. The crystal structures of several DUS proteins have been determined: those of *Thermus thermophilus* DUS in complex with tRNA or a D-loop-containing small RNA substrate (Yu et al., 2011), *E. coli* DusC, alone (Chen et al., 2013) or in complex with tRNA (Byrne et al., 2015), *E. coli* DusB alone (Bou-Nader et al., 2018) and protein TM0096 from *Thermotoga maritima* (Park et al., 2004), which was not biochemically characterized. Compared to the bacterial enzymes, which are composed of a catalytic domain and a tRNA recognition domain, the human enzyme hDus2 possesses an additional C-terminal dsRBD. The structure of a construct of hDus2 comprising the first two N-terminal domains has been solved both using Se-SAD phasing (Whelan et al., 2015) and by molecular replacement (Bou-Nader et al., 2015; Whelan et al., 2015), the fold of this region being sufficiently conserved between species despite a low sequence identity (18%) (Griffiths et al., 2012). The dsRBD is a 65–70 amino acids domain present in proteins involved in various biological processes such as antiviral response, mRNA editing, RNA processing, RNA transport or gene silencing through RNA interference (Fierro-Monti and Mathews, 2000; Saunders and Barber, 2003; Tian et al., 2004). The dsRBDs fold is conserved despite large sequence variations (Gleghorn and Maquat, 2014); however, no crystal structure in the PDB presented sufficient sequence similarity to be used for molecular replacement. We have previously reported the structure of the dsRBD domain of hDus2 together with functional studies of the individual domains and the full-length protein (Bou-Nader et al., 2015). We detail here the data collection strategies and sulfur-SAD phasing methods that were used to solve the dsRBD structure.

The hdus2 dsRBD construct used in this work contains 3 cysteines and 2 methionines (apart from the possible N-terminal methionine) i. e. a sulfur content of 4.2%, which is the average value for eukaryotic proteins (Jauregui et al., 2000). The dsRBD crystals had tetragonal symmetry, 3 molecules in the asymmetric unit and a modest solvent content of 41.8%. Thus, the contribution of solvent flattening to resolve the phase ambiguity was not expected to be very important. The crystals diffracted well, up to 1.77 Å resolution at λ = 0.98 Å. At a wavelength of 1.8 Å (f' = 0.7412), the anomalous signal estimated by the expected Bijvoet ratio (<ΔF>/<F>) (Hendrickson and Teet, 1981) was 1.08%. This value is lower than the average ratio of 1.4% estimated for proteins for which the structure was solved by native SAD (Rose et al., 2015), but well above the current limit of 0.46% (Wang et al., 2006), which indicated that sulfur-SAD phasing should be feasible.

Because of the high diffracting power of the crystals, several highly redundant data sets were collected on a single crystal at the PROXIMA1 beamline at the SOLEIL synchrotron at different κ angles with ϕ or ω as the rotation axis using the three-circle κ-geometry goniostat (Table 2). To find the optimized combination of high data redundancy and low radiation damage, we compared data sets from four crystals (named D1, D5, D6, D7) collected at different X-ray doses (beam transmission of 50, 40, 20 and 5%, respectively, compared to the data set collected at λ = 0.98 Å) (Tables 2 and 3). For the merged data sets corresponding to each of the four crystals, the amounts of anomalous signal <ΔF>/σ <F> as a function of resolution are shown in Fig. 1A. These curves show a significant increase of the anomalous signal at low resolution for the two crystals (D6 and D7) for which the incident beam intensity was highly reduced. In these cases, more images could be collected, which resulted both in much higher redundancies (multiplicities of 21.3 and 34.0) and higher signal-to-noise ratios (I/σ(I) of 61.4 and 62.7) (Table 3).

Table 3
Data collection and reduction statistics of the merged data for the four crystals and structure determination parameters. Values in parentheses correspond to the highest resolution shell, unless otherwise indicated.

Crystal	D1	D5	D6	D7
Resolution (Å)	50–2.2 (2.33–2.2)	50–2.2 (2.33–2.2)	50–2.2 (2.33–2.2)	50–2.2 (2.33–2.2)
Multiplicity	9.5 (7.7)	9.3 (7.6)	21.3 (18.5)	34.0 (29.3)
Completeness (%)	100 (100)	99.9 (99.5)	100 (99.1)	99.9 (99.0)
R_{meas}	5.2 (23.9)	6.5 (21.5)	4.3 (23.8)	5.1 (14.3)
I/σ(I)	32.5 (10.8)	25.9 (9.9)	61.4 (12.9)	62.7 (24.2)
ΔF/σ(ΔF)	1.51 (1.05)	2.35 (1.43)	1.40 (0.87)	1.50 (1.01)
ΔF/σ(ΔF) 50–2.9 Å (2.98–2.9 Å)	2.04 (1.7)	2.85 (2.85)	1.95 (1.24)	1.92 (1.44)
Anomalous Corr (%)	43 (27)	73 (48)	28 (10)	44 (18)
Anomalous Corr (%) 50–2.9 Å (2.98–2.9 Å)	66 (54)	85 (80)	57 (33)	71 (52)
Best CC_{all}/CC_{weak} (shelxd)[a]	22.2/11.7	15.7/6.7	35.9/20.1	42.2/24.0
pseudofree_CC original/inverted (%) (shelxe)	49.2/48.8	43.2/43.8	58.7/70.5	59.7/69.7
Structure solved by shelxd/shelxe	No	No	Yes	Yes

[a] Data were truncated to 2.9 Å (D1, D5) or 2.2 Å (D6, D7).

SHELXD was used to solve the substructure using data truncated to 2.9 Å (crystals D1 and D5) or 2.2 Å (crystals D6 and D7), with the resolution cut-off corresponding to an anomalous signal <ΔF>/<σ(ΔF)> higher than 1.0 (Fig. 1A). 14 S atoms out of 15 were successfully located with occupation factors greater than 0.5, for the D6 and D7 crystals. Success of substructure determination was demonstrated by the histograms showing 230 and 360 correct solutions with CC_{all} = 36% or 42% (CC_{all} is the correlation coefficient between all normalized structure factor differences in the measured data and those calculated from a given substructure solution), for D6 and D7, respectively, out of 500 trials (Fig. 1C). A clean separation of correct solutions from non-correct solutions was observed. Moreover, for both crystals D6 and D7, the correct sulfur positions were found with data truncated to any range between 2.2 and 3.5 Å resolution (data not shown). The D6 and D7 data sets led also to successful phasing, as shown by the contrast between the two enantiomorphs during *SHELXE* density modification (Fig. 1D), which indicates that the inverted heavy-atom substructure is the correct one. The contrast between the two possible solutions was similar for the D7 and D6 data (Fig. 1D). Both data sets allowed straightforward automated model building at 2.2 Å (Fig. 2A). For the D7 data set, 75% of the residues were built by *SHELXE*, with the polypeptide chain being almost completely correctly traced.

In contrast, for the D1 and D5 data, only 4 or 8 sulfur sites, respectively, had an occupancy higher than 0.5 (Fig. 1B) and the histograms show that no successful solution with increased CC_{all} value emerges from non-solutions (Fig. 1C), indicating random substructure positioning. Unsuccessful structure solving was confirmed by the absence of contrast between the two possible enantiomers when phases were calculated in *SHELXE* (Fig. 1D).

Interestingly, although the overall anomalous signals <ΔF>/

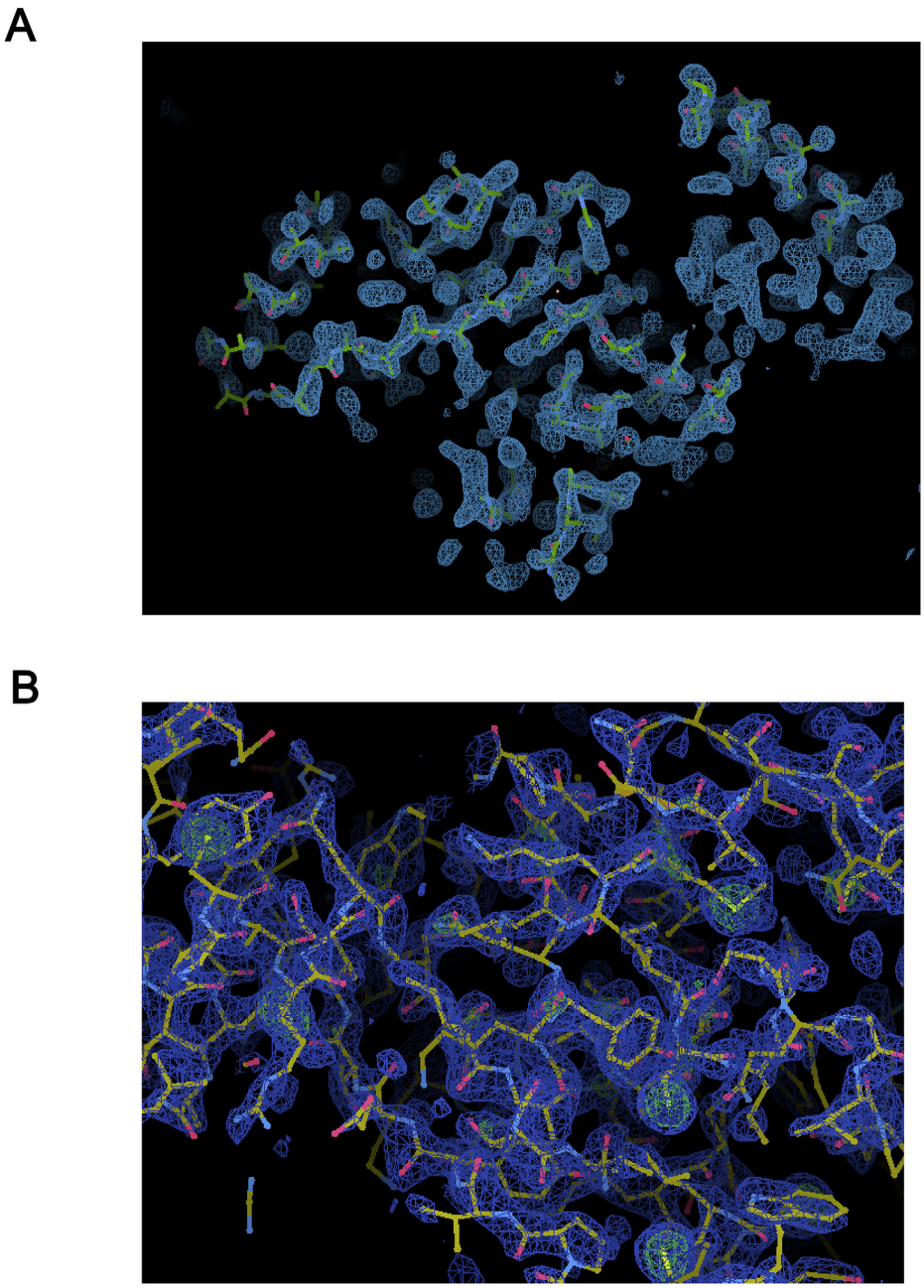

Fig. 2. Initial electron density map at 2.2 Å (inverted hand) contoured at the level of 1.5 σ obtained from *SHELXE* showing the chain fragments (stick representation) built after 3 cycles of autotracing (crystal D7). **B** Solvent-flattened experimental electron-density map contoured at 2 σ (blue mesh) and 3 σ (green mesh highlighting the sulfur atoms), with the model automatically built by *BUCCANEER* in stick representation.

<σ(ΔF)> calculated from D6 and D7 data were lower compared to those from D1 and D5 data sets (Table 3), the latter were not suitable for phasing. The higher signal-to-ratio values of D6 and D7 data sets is also noticeable, indicating the better accuracy of the estimated intensities and anomalous signal values. The substructure could be determined using the data up to 2.2 Å resolution, where ΔF/σ(ΔF) in the last resolution shell was 0.9–1.0 (with ΔF/σ(ΔF) of 1.4–1.5 for all data), indicating that the "rule" ΔF/σ(ΔF) >1.5 in all resolution ranges was not a necessary requirement for sulfur SAD substructure location, in contrast to other cases (Cianci et al., 2008).

The substructure determined from D6 and D7 data sets was refined and completed (one more sulfur site found) with *PHASER*, which also produced electron density maps that were subsequently modified by solvent flattening with *PARROT*. An easily interpretable electron-density map was obtained (Fig. 2B). The structure was successfully traced by *BUCCANEER* with, for D7, correct building during the first cycle of 257 residues (91% of the final structure) in 4 chains, the longest having 91 residues. After 5 cycles, the structure was 99% complete and refined to R_{work} and R_{free} values of 24.6 and 27.8%, respectively. Further building was done manually with *COOT* (Emsley et al., 2010) and refinement with *REFMAC5* (Murshudov et al., 2011). The statistics for the refined crystal structure and structural analysis of the dsRBD have previously been reported (Bou-Nader et al., 2015).

4. Conclusion

Proteins contain cysteine and methionine residues, whose sulfur atoms can be used for native phasing in the absence of exogenous anomalous scatterers. Yet, radiation damage in protein crystals is primarily located at the sulfur sites, and both specific and non-specific radiation damage degrade the anomalous signal. To get the best accurate measurements of the weak anomalous signal of sulfur in the hDus2 dsRBD crystals, variations in the incident beam intensity were studied. SAD-data sets were collected up to 2.2 Å resolution on a single well-diffracting crystal, which allowed us to get rid of crystal variations (in unit cells, overall diffraction, anomalous correlation coefficient) that occur when scaling multiple crystals. Highly redundant data sets (multiplicity of 3–9 per orientation) were obtained by rotating the crystal along the ϕ or ω axis with fixed κ angle. An appropriate combination of high multiplicity and weak radiation damage was reached by using a highly attenuated beam (20% or 5% transmission compared to the data set collected at higher energy), ensuring a high signal-to-noise ratio and an accurate estimation of the anomalous signal. We consider that there is no unambiguous indicator, which is capable of predicting the final success of S-SAD solving, especially in more challenging cases. While the Bijvoet ratio for the DUS dsRBD crystals was lower than average, the high diffracting power and the tetragonal symmetry of the crystals were advantageous for S-SAD phasing. Our successful example together with a review of structures solved by SAD phasing using sulfur as the unique anomalous scatterer should help non-expert crystallographers to plan a sulfur-SAD experiment for proteins crystals diffracting better than ~3 Å.

CRediT authorship contribution statement

Beatriz Gomes Guimarães: Conceptualization, Methodology, Software, Formal analysis, Data curation, Writing – review & editing. **Béatrice Golinelli-Pimpaneau:** Investigation, Writing – original draft, Writing – review & editing, Visualization.

Declaration of competing interest

The authors declare that they have no known competing financial interests or personal relationships that could have appeared to influence the work reported in this paper.

Acknowledgements

We acknowledge the use of beamline PROXIMA 1 at the SOLEIL synchrotron, Saint Aubin, France and thank Pierre Legrand and Andrew Thompson from PROXIMA 1 for their help in data analysis and structure determination.

References

Adams, P.D., Afonine, P.V., Bunkoczi, G., Chen, V.B., Davis, I.W., Echols, N., Headd, J.J., Hung, L.W., Kapral, G.J., Grosse-Kunstleve, R.W., McCoy, A.J., Moriarty, N.W., Oeffner, R., Read, R.J., Richardson, D.C., Richardson, J.S., Terwilliger, T.C., Zwart, P.H., 2010. PHENIX: a comprehensive Python-based system for macromolecular structure solution. Acta Crystallogr D Biol Crystallogr 66, 213–221.

Akey, D.L., Brown, W.C., Konwerski, J.R., Ogata, C.M., Smith, J.L., 2014. Use of massively multiple merged data for low-resolution S-SAD phasing and refinement of flavivirus NS1. Acta Crystallogr D Biol Crystallogr 70, 2719–2729.

Assmann, G.M., Wang, M., Diederichs, K., 2020. Making a difference in multi-data-set crystallography: simple and deterministic data-scaling/selection methods. Acta Crystallogr D Biol Crystallogr 76, 636–652.

Banerjee, S., Coussens, N.P., Gallat, F., Sathyanarayanan, N., Srikanth, J., Yagi, K.J., Gray, J.S., Tobe, S.S., Stay, B., Chavas, L.M., Ramaswamy, S., 2016. Structure of a heterogeneous, glycosylated, lipid-bound, in vivo-grown protein crystal at atomic resolution from the viviparous cockroach *Diploptera punctata*. IUCrJ 3, 282–293.

Banumathi, S., Dauter, M., Dauter, Z., 2003. Phasing at high resolution using Ta6Br12 cluster. Acta Crystallogr D Biol Crystallogr 59, 492–498.

Basu, S., Finke, A., Vera, L., Wang, M., Olieric, V., 2019a. Making routine native SAD a reality: lessons from beamline X06DA at the Swiss Light Source. Acta Crystallogr D Biol Crystallogr 75, 262–271.

Basu, S., Olieric, V., Leonarski, F., Matsugaki, N., Kawano, Y., Takashi, T., Huang, C.-Y., Yamada, Y., Vera, L., Olieric, N., Basquin, J., Wojdyla, J.A., Bunk, O., Diederichs, K., Yamamotoc, M., Wang, M., 2019b. Long-wavelength native-SAD phasing: opportunities and challenges. IUCrJ. 6, 373–386.

Bou-Nader, C., Pecqueur, L., Bregeon, D., Kamah, A., Guerineau, V., Golinelli-Pimpaneau, B., Guimaraes, B.G., Fontecave, M., Hamdane, D., 2015. An extended dsRBD is required for post-transcriptional modification in human tRNAs. Nucleic Acids Res. 43, 9446–9456.

Bou-Nader, C., Montemont, H., Guerineau, V., Jean-Jean, O., Bregeon, D., Hamdane, D., 2018. Unveiling structural and functional divergences of bacterial tRNA dihydrouridine synthases: perspectives on the evolution scenario. Nucleic Acids Res. 46, 1386–1394.

Broennimann, C., Eikenberry, E.F., Henrich, B., Horisberger, R., Huelsen, G., Pohl, E., Schmitt, B., Schulze-Briese, C., Suzuki, M., Tomizaki, T., Toyokawa, H., Wagner, A., 2006. The PILATUS 1M detector. J. Synchrotron Radiat. 13, 120–130.

Byrne, R.T., Jenkins, H.T., Peters, D.T., Whelan, F., Stowell, J., Aziz, N., Kasatsky, P., Rodnina, M.V., Koonin, E.V., Konevega, A.L., Antson, A.A., 2015. Major reorientation of tRNA substrates defines specificity of dihydrouridine synthases. Proc. Natl. Acad. Sci. U. S. A. 112, 6033–6037.

Chen, M., Yu, J., Tanaka, Y., Tanaka, M., Tanaka, I., Yao, M., 2013. Structure of dihydrouridine synthase C (DusC) from *Escherichia coli*. Acta Crystallogr Sect F Struct Biol Cryst Commun 69, 834–838.

Cianci, M., Helliwell, J.R., Suzuki, A., 2008. The interdependence of wavelength, redundancy and dose in sulfur SAD experiments. Acta Crystallogr D Biol Crystallogr 64, 1196–1209.

Cianci, M., Groves, M.R., Barford, D., Schneider, T.R., 2016. Data collection with a tailored X-ray beam size at 2.69 Å wavelength (4.6 keV): sulfur SAD phasing of Cdc23(Nterm). Acta Crystallogr D Struct Biol 72, 403–412.

Cianci, M., Bourenkov, G., Pompidor, G., Karpics, I., Kallio, J., Bento, I., Roessle, M., Cipriani, F., Fiedler, S., Schneider, T.R., 2017. P13, the EMBL macromolecular crystallography beamline at the low-emittance PETRA III ring for high- and low-energy phasing with variable beam focusing. J. Synchrotron Radiat. 24, 323–332.

Cianci, M., Nanao, M., Schneider, T.R., 2019. Long-wavelength Mesh&Collect native SAD phasing from microcrystals. Acta Crystallogr D Struct Biol 75, 192–199.

Cowtan, K., 2006. The Buccaneer software for automated model building. 1. Tracing protein chains. Acta Crystallogr D Biol Crystallogr 62, 1002–1011.

Cowtan, K., 2010. Recent developments in classical density modification. Acta Crystallogr D Biol Crystallogr 66, 470–478.

Dauter, Z., Dauter, M., de La Fortelle, E., Bricogne, G., Sheldrick, G.M., 1999. Can anomalous signal of sulfur become a tool for solving protein crystal structures? J. Mol. Biol. 289, 83–92.

De Sanctis, D., Oscarsson, M., Popov, A., Svensson, O., Leonard, G., 2016. Facilitating best practices in collecting anomalous scattering data for de novo structure solution at the ESRF Structural Biology Beamlines. Acta Crystallogr D Biol Crystallogr 72, 413–420.

Doutch, J., Hough, M.A., Hasnain, S.S., Strange, R.W., 2012. Challenges of sulfur SAD phasing as a routine method in macromolecular crystallography. J. Synchrotron Radiat. 19, 19–29.

El Omari, K., Iourin, O., Kadlec, J., Fearn, R., Hall, D.R., Harlos, K., Grimes, J.M., Stuart, D.I., 2014. Pushing the limits of sulfur SAD phasing: *de novo* structure solution of the N-terminal domain of the ectodomain of HCV E1. Acta Crystallogr D Biol Crystallogr 70, 2197–2203.

Emsley, P., Lohkamp, B., Scott, W.G., Cowtan, K., 2010. Features and development of coot. Acta Crystallogr D Biol Crystallogr 66, 486–501.

Fierro-Monti, I., Mathews, M.B., 2000. Proteins binding to duplexed RNA: one motif, multiple functions. Trends Biochem. Sci. 25, 241–246.
Foos, N., Cianci, M., Nanao, M.H., 2019. Choosing your (Friedel) mates wisely: grouping data sets to improve anomalous signal. Acta Crystallogr D Struct Biol 75, 200–210.
Gleghorn, M.L., Maquat, L.E., 2014. 'Black sheep' that don't leave the double-stranded RNA-binding domain fold. Trends Biochem. Sci. 39, 328–340.
Gorgel, M., Boggild, A., Ulstrup, J.J., Weiss, M.S., Müller, U., Nissen, P., Boesen, T., 2015. Against the odds? De novo structure determination of a pilin with two cysteine residues by sulfur SAD. Acta Crystallogr D Biol Crystallogr 71, 1095–1101.
Goulet, A., Vestergaard, G., Felisberto-Rodrigues, C., Campanacci, V., Garrett, R.A., Cambillau, C., Ortiz-Lombardia, M., 2010. Getting the best out of long-wavelength X-rays: de novo chlorine/sulfur SAD phasing of a structural protein from ATV. Acta Crystallogr D Biol Crystallogr 66, 304–308.
Griffiths, S., Byrne, R.T., Antson, A.A., Whelan, F., 2012. Crystallization and preliminary X-ray crystallographic analysis of the catalytic domain of human dihydrouridine synthase. Acta Crystallogr Sect F Struct Biol Cryst Commun 68, 333–336.
Guo, G., Zhu, P., Fuchs, M.R., Shi, W., Andi, B., Gao, Y., Hendrickson, W.A., McSweeney, S., Liu, Q., 2019. Synchrotron microcrystal native-SAD phasing at a low energy. IUCrJ 6, 532–542.
Hegde, R.P., Fedorov, A.A., Sauder, J.M., Burley, S.K., Almob, S.C., Ramagopal, U.A., 2017. The hidden treasure in your data: phasing with unexpected weak anomalous scatterers from routine data sets. Acta Crystallogr Sect F Struct Biol Cryst Commun 73, 184–195.
Hendrickson, W.A., 1991. Determination of macromolecular structures from anomalous diffraction of synchrotron radiation. Science 254, 51–58.
Hendrickson, W.A., 2014. Anomalous diffraction in crystallographic phase evaluation. Q. Rev. Biophys. 47, 49–93.
Hendrickson, W.A., Teet, M.M., 1981. Structure of the hydrophobic protein crambin determined directly from the anomalous scattering of sulfur. Nature 290, 107–113.
Jauregui, R., Bolivar, F., Merino, E., 2000. Relationship between whole proteome aminoacid composition and static DNA curvature. Microb. Comp. Genom. 5, 7–15.
Kabsch, W., 2010. Xds. Acta Crystallogr D Biol Crystallogr 66, 125–132.
Klinke, S., Foos, N., Rinaldi, J.J., Paris, G., Goldbaum, F.A., Legrand, P., Guimaraes, B.G., Thompson, A., 2015. S-SAD phasing of monoclinic histidine kinase from *Brucella abortus* combining data from multiple crystals and orientations: an example of datacollection strategy and a posteriori analysis of different data combinations. Acta Crystallogr D Biol Crystallogr 71, 1433–1443.
Kraatz, S.H.W., Bianchi, S., Steinmetz, M.O., 2018. Combinatorial use of disulfide bridges and native sulfur-SAD phasing for rapid structure determination of coiled-coils. Biosci. Rep. 38, BSR20181073.
Liebschner, D., Yamada, Y., Matsugaki, N., Senda, M., Senda, T., 2016. On the influence of crystal size and wavelength on native SAD phasing. Acta Crystallogr D Struct Biol 72, 728–741.
Liu, Q., Hendrickson, W.A., 2015. Crystallographic phasing from weak anomalous signals. Cur Op Struct Biol 34, 99–107.
Liu, Q., Dahmane, T., Zhang, Z., Assur, Z., Brasch, J., Shapiro, L., Mancia, F., Hendrickson, W.A., 2012. Structures from anomalous diffraction of native biological macromolecules. Science 336, 1033–1037.
Liu, Q., Guo, Y., Chang, Y., Cai, Z., Assur, Z., Mancia, F., Greene, M.I., Hendrickson, W.A., 2014. Multi-crystal native SAD analysis at 6keV. Acta Crystallogr D Biol Crystallogr 70, 2544–2557.
Mueller-Dieckmann, C., Panjikar, S., Schmidt, A., Mueller, S., Kuper, J., Geerlof, A., Wilmanns, M., Singh, R.K., Tucker, P.A., Weiss, M.S., 2007. On the routine use of soft X-rays in macromolecular crystallography. Part IV. Efficient determination of anomalous substructures in biomacromolecules using longer X-ray wavelengths. Acta Crystallogr D Biol Crystallogr 63, 366–380.
Murshudov, G.N., Skubák, P., Lebedev, A.A., Pannu, N.S., Steiner, R.A., Nicholls, R.A., Winn, M.D., Long, F., Vagin, A.A., 2011. REFMAC5 for the refinement of macromolecular crystal structures. Acta Crystallogr D Biol Crystallogr 67, 355–367.
Nass, K., Cheng, R., Vera, L., Mozzanica, A., Redford, S., Ozerov, D., Basu, S., James, D., Knopp, G., Cirelli, C., Martiel, I., Casadei, C., Weinert, T., Nogly, P., Skopintsev, P., Usov, I., Leonarski, F., Geng, T., Rappas, M., Doré, A.S., Cooke, R., Nasrollahi Shirazi, S., Dworkowski, F., Sharpe, M., Olieric, N., Bacellar, C., Bohinc, R., Steinmetz, M.O., Schertler, G., Abela, R., Patthey, L., Schmitt, B., Hennig, M., Standfuss, J., Wang, M., Milne, C.J., 2020. Advances in long-wavelength native phasing at X-ray free-electron lasers. IUCrJ 7, 965–975.
Nawrotek, A., Guimaraes, B.G., Velours, C., Subtil, A., Knossow, M., Gigant, B., 2014. Biochemical and structural insights into microtubule perturbation by CopN from *Chlamydia pneumoniae*. J. Biol. Chem. 289, 25199–25210.
Olczak, A., Cianci, M., 2018. The signal-to-noise ratio in SAD experiments. Crystallogr. Rev. 24 (2), 73–101.
Olieric, V., Weinert, T., Finke, A.D., Anders, C., Li, D., Olieric, N., Borca, C.N., Steinmetz, M.O., Caffrey, M., Jinek, M., Wang, M., 2016. Data-collection strategy for challenging native SAD phasing. Acta Crystallogr D Biol Crystallogr 72, 421–429.
Pape, T., Schneider, T.R., 2004. HKL2MAP: a graphical user interface for macromolecular phasing with SHELX programs. J. Appl. Crystallogr. 37, 843–844.
Park, F., Gajiwala, K., Noland, B., Wu, L., He, D., Molinari, J., Loomis, K., Pagarigan, B., Kearins, P., Christopher, J., Peat, T., Badger, J., Hendle, J., Lin, J., Buchanan, S., 2004. The 1.59 A resolution crystal structure of TM0096, a flavin mononucleotide binding protein from *Thermotoga maritima*. Proteins 55, 772–774.
Ramagopal, U.A., Dauter, M., Dauter, Z., 2003. Phasing on anomalous signal of sulfurs: what is the limit? Acta Crystallogr D Biol Crystallogr 59, 1020–1027.
Rose, J.P., Bi-Cheng Wang, B.-C., Weiss, M.S., 2015. Native SAD is maturing. IUCrJ 2, 431–440.
Sarma, G.N., Karplus, P.A., 2006. In-house sulfur SAD phasing: a case study of the effects of data quality and resolution cutoffs. Acta Crystallogr D Biol Crystallogr 62, 707–716.
Saunders, L.R., Barber, G.N., 2003. The dsRNA binding protein family: critical roles, diverse cellular functions. Faseb. J. 17, 961–983.
Schneider, T.R., Sheldrick, G.M., 2002. Substructure solution with SHELXD. Acta Crystallogr D Biol Crystallogr 58, 1772–1779.
Sheldrick, G.M., 2002. Macromolecular phasing with SHELXE. Z. Kristallogr. 217, 644–650.
Shi, K., Kurniawan, F., Banerjee, S., Moeller, N.H., Aihara, H., 2020. Crystal structure of bacteriophage T4 Spackle as determined by native SAD phasing. Acta Crystallogr D Biol Crystallogr 76, 899–904.
Sun, X., Ye, Y., Sakurai, N., Koji Kato, Yuasa K., Tsuji, A., Yao, M., 2020. Crystallographic analysis of *Eisenia* hydrolysis enhancing protein using a long wavelength for native-SAD phasing. Acta Crystallogr Sect F Struct Biol Cryst Commun 76, 20–24.
Tian, B., Bevilacqua, P.C., Diegelman-Parente, A., Mathews, M.B., 2004. The double-stranded-RNA-binding motif: interference and much more. Nat. Rev. Mol. Cell Biol. 5, 1013–1023.
Usón, I., Sheldrick, G.M., 2018. An introduction to experimental phasing of macromolecules illustrated by SHELX; new autotracing features. Acta Crystallogr D Struct Biol 74, 106–116.
Vasur, J., Kawai, R., Larsson, A.M., Igarashi, K., Sandgren, M., Samejima, M., Stahlberg, J., 2006. X-ray crystallographic native sulfur SAD structure determination of laminarinase Lam16A from *Phanerochaete chrysosporium*. Acta Crystallogr D Biol Crystallogr 62, 1422–1429.
Wang, J., Dauter, M., Dauter, Z., 2006. What can be done with a good crystal and an accurate beamline? Acta Crystallogr D Biol Crystallogr 62, 1475–1483.
Watanabe, N., 2006. From phasing to structure refinement in-house: Cr/Cu dual-wavelength system and a loopless free crystal-mounting method. Acta Crystallogr D Biol Crystallogr 62, 891–896.
Weinert, T., Olieric, V., Waltersperger, S., Panepucci, E., Chen, L., Zhang, H., Zhou, D., Rose, J., Ebihara, A., Kuramitsu, S., Li, D., Howe, N., Schnapp, G., Pautsch, A., Bargsten, K., Prota, A.E., Surana, P., Kottur, J., Nair, D.T., Basilico, F., Cecatiello, V., Pasqualato, S., Boland, A., Weichenrieder, O., Wang, B.C., Steinmetz, M.O., Caffrey, M., Wang, M., 2015. Fast native-SAD phasing for routine macromolecular structure determination. Nat. Methods 12, 131–133.
Whelan, F., Jenkins, H.T., Griffiths, S.C., Byrne, R.T., Dodson, E.J., Antson, A.A., 2015. From bacterial to human dihydrouridine synthase: automated structure determination. Acta Crystallogr D Biol Crystallogr 71, 1564–1571.
Yu, F., Tanaka, Y., Yamashita, K., Suzuki, T., Nakamura, A., Hirano, N., Yao, M., Tanaka, I., 2011. Molecular basis of dihydrouridine formation on tRNA. Proc. Natl. Acad. Sci. U. S. A. 108, 19593–19598.
Yu, J., Shinoda, A., Kato, K., Tanaka, I., Yao, M., 2020. A solution-free crystal-mounting platform for native SAD. Acta Crystallogr D Biol Crystallogr 76, 938–945.
Zhu, J.Y., Fu, Z.Q., Chen, L., Xu, H., Chrzas, J., Rose, J., Wang, B.C., 2012. Structure of the *Archaeoglobus fulgidus* orphan ORF AF1382 determined by sulfur SAD from a moderately diffracting crystal. Acta Crystallogr D Biol Crystallogr 68, 1242–1252.